Acta Pharmaceutica Sinica B 2024;14(1):392–404

Chinese Pharmaceutical Association
Institute of Materia Medica, Chinese Academy of Medical Sciences

Acta Pharmaceutica Sinica B

www.elsevier.com/locate/apsb
www.sciencedirect.com

ORIGINAL ARTICLE

# Visualization of nasal powder distribution using biomimetic human nasal cavity model

**Jiawen Su[a,e], Yan Liu[f], Hongyu Sun[c], Abid Naeem[a], Huipeng Xu[c], Yue Qu[f], Caifen Wang[c,f], Zeru Li[c,h], Jianhua Lu[d], Lulu Wang[g], Xiaofeng Wang[g], Jie Wu[d,e], Lixin Sun[f], Jiwen Zhang[a,b,c,e], Zhigang Wang[d,*], Rui Yang[f,g,*], Li Wu[a,b,c,e,*]**

[a]*Key Laboratory of Modern Preparation of TCM, Ministry of Education, Jiangxi University of Chinese Medicine, Nanchang 330004, China*
[b]*Key Laboratory of Molecular Pharmacology and Drug Evaluation, School of Pharmacy, Ministry of Education, Yantai University, Yantai 264005, China*
[c]*Shanghai Institute of Materia Medica, Chinese Academy of Sciences, Shanghai 201210, China*
[d]*Nantong Haimen People's Hospital, Nantong 226199, China*
[e]*Yangtze Delta Drug Advanced Research Institute, Nantong 226126, China*
[f]*Shenyang Pharmaceutical University, Shenyang 110016, China*
[g]*National Institutes for Food and Drug Control, Beijing 100000, China*
[h]*Nanjing University of Chinese Medicine, Nanjing 210023, China*

Received 29 March 2023; received in revised form 9 May 2023; accepted 19 May 2023

**KEY WORDS**

Nasal drug deposition;
Nasal drug distribution;
Nasal drug delivery;
Biomimetic nasal model;
Nasal powder;
Three-dimensional reconstruction;
Three-dimensional printing;
Nasal drug distribution

**Abstract** Nasal drug delivery efficiency is highly dependent on the position in which the drug is deposited in the nasal cavity. However, no reliable method is currently available to assess its impact on delivery performance. In this study, a biomimetic nasal model based on three-dimensional (3D) reconstruction and three-dimensional printing (3DP) technology was developed for visualizing the deposition of drug powders in the nasal cavity. The results showed significant differences in cavity area and volume and powder distribution in the anterior part of the biomimetic nasal model of Chinese males and females. The nasal cavity model was modified with dimethicone and validated to be suitable for the deposition test. The experimental device produced the most satisfactory results with five spray times. Furthermore, particle sizes and spray angles were found to significantly affect the experimental device's performance and alter drug distribution, respectively. Additionally, mometasone furoate (MF) nasal spray (NS) distribution patterns were investigated in a goat nasal cavity model and three male goat noses, confirming the *in vitro* and

*Corresponding authors.
E-mail addresses: hmrywzg@sina.com (Zhigang Wang), yangr@nifdc.org.cn (Rui Yang), wuli@simm.ac.cn (Li Wu).
Peer review under the responsibility of Chinese Pharmaceutical Association and Institute of Materia Medica, Chinese Academy of Medical Sciences.

https://doi.org/10.1016/j.apsb.2023.06.007

visualization

*in vivo* correlation. In conclusion, the developed human nasal structure biomimetic device has the potential to be a valuable tool for assessing nasal drug delivery system deposition and distribution.



## 1. Introduction

Nasal drug administration has been practiced in the Indian and traditional Chinese medical systems for centuries[1]. Nasal administration was first reported in the early 1980s as a potential alternative route for systemic delivery instead of conventional routes. Nowadays, nasal drug administration is widely used to treat local upper respiratory tract diseases, such as nasal congestion, nasal infections, and nasal allergic diseases[2,3]. In recent years, nasal administration has also been considered for systemic delivery[4–6], mucosal vaccination[7,8], and nose-to-brain delivery[9–15]. Nasal drug administration has numerous advantages[16,17], such as large absorption surface area, rapid drug absorption, no hepatic first-pass metabolism, high bioavailability, fast onset of action, direct access to the central nervous system along the olfactory nerves, and shows good patient compliance[18,19]. As a convenient and reliable route for the local and systemic administration of drugs, recent research efforts have focused on developing novel nasal delivery systems[20–22]. In order to optimize and improve the efficacy of nasal drug administration, different types of nasal drug delivery systems have been developed[17]. These include nasal drops and sprays, nasal gels, nasal suspensions and emulsions, nasal micellar and liposomal formulations, nasal powders, and nasal particles, among which nasal powders are a particularly effective formulation[23]. Firstly, the drug in nasal powders is kept in a solid state to endow it with better chemical stability compared to liquid or semi-liquid formulations. Secondly, preservatives are not required in nasal powders to avoid their irritative effect, as in liquid and semi-solid formulations. Finally, powder systems are capable of administering larger doses of drugs for high loading and strength of the drug.

Although nasal drug administration has numerous advantages, it can only be achieved when the drug particles or mists are deposited in the right regions of the nasal cavities. Thus, evaluating the nasal deposition and distribution profile of nasal formulations is of enormous significance. However, there are still no appropriate recommendations or guidelines for nasal deposition studies[24]. Currently, deposition studies in nasal cavities are performed *in vitro* using nasal casts or computational fluid dynamics simulations. A few studies have exploited transparent nasal casts to evaluate the deposition pattern of nasal formulations. Kundoor et al.[25] established a straightforward and inexpensive method to evaluate the deposition pattern of nasal spray directly. The transparent nasal cavities were uniformly applied with Sar-Gel® that changed colors upon contact with water, and the deposition pattern was captured using a digital camera. Inspired by this innovative method, several studies were also conducted based on this color-based method[26,27]. However, the color-based method has some inherent drawbacks. Its sensitivity is low, and it leads to errors when quantitative analysis is required. Besides, water is essential in this method, which hinders its application to nasal powders. Furthermore, the gels coated on the surface of nasal cavities might bring in uncontrollable effects in experiments, and artificial mucus cannot be applied simultaneously. Hence, a fluorescence-based method was developed to visualize and quantify the deposition pattern of nasal powders in a transparent nasal cast.

In this study, the digital nasal model was first developed utilizing computed tomography (CT) data from Chinese adult males and females to select the nasal cavity closest to the average cavity area and volume. Then the biomimetic nasal cast was fabricated by the three-dimensional printing (3DP) technique based on the digital nasal model. Only a limited number of nasal powders are approved for use abroad, and none are available domestically. Cyclodextrin metal−organic frameworks (CD-MOFs) with strictly uniform sizes and cubic shapes with controllable properties have been extensively studied in our laboratory as drug carriers for dry powder inhalers (DPI)[28,29]. Therefore, CD-MOFs were selected as the standard/model preparation in this study. The physical mixture of Rhodamine B (RhoB) and CD-MOFs was used to obtain fluorescent RhoB@MOFs, for observing and analyzing deposition patterns. Subsequently, the influence of spray angles, spray times, particle sizes, and coating solutions on nasal deposition patterns were evaluated. Specifically, the effect of gender, which was commonly ignored in other studies, was studied in detail. In order to prove the reliability of the method to evaluate nasal preparations through three-dimensional reconstruction of biomimetic model, mometasone furoate (MF) nasal spray (NS) was selected as the standard preparation in this research. A goat nasal evaluation model was constructed using head and neck CT of a male goat. Drug distribution experiments were conducted to demonstrate a drug deposition correlation between the goat nasal cavity model (*in vitro*) and the goat nose (*in vivo*). In a nutshell, a biomimetic human nasal cavity model was utilized to visualize the nasal powder distribution and precise quantification of deposited powders in the nasal cavity based on the fluorescent intensities of the powders (Scheme 1).

## 2. Materials and methods

### 2.1. Materials

The analysis of head and neck CTs data of adults with no previous respiratory history were approved by the Ethics Committee of Nantong Haimen People's Hospital (Ethical approval number: 2023-YJKY001). Briefly, the CT data of 32 subjects, namely, 16 Chinese males and 16 Chinese females, ranging in age from 20 to 59 years old were processed to generate a standardized nasal cavity structure of Chinese subjects. Inclusion criteria: CTs showed no deviation of the nasal septum, no mucosal edema, and no turbinate hypertrophy, age from 20 to 59. Exclusion criteria: patients with allergic rhinitis, nasal tumors, severe nasal trauma and postoperative nasal sinus diseases. The interval distances between two consecutive CT images ranged from 0.7 mm to 1 mm

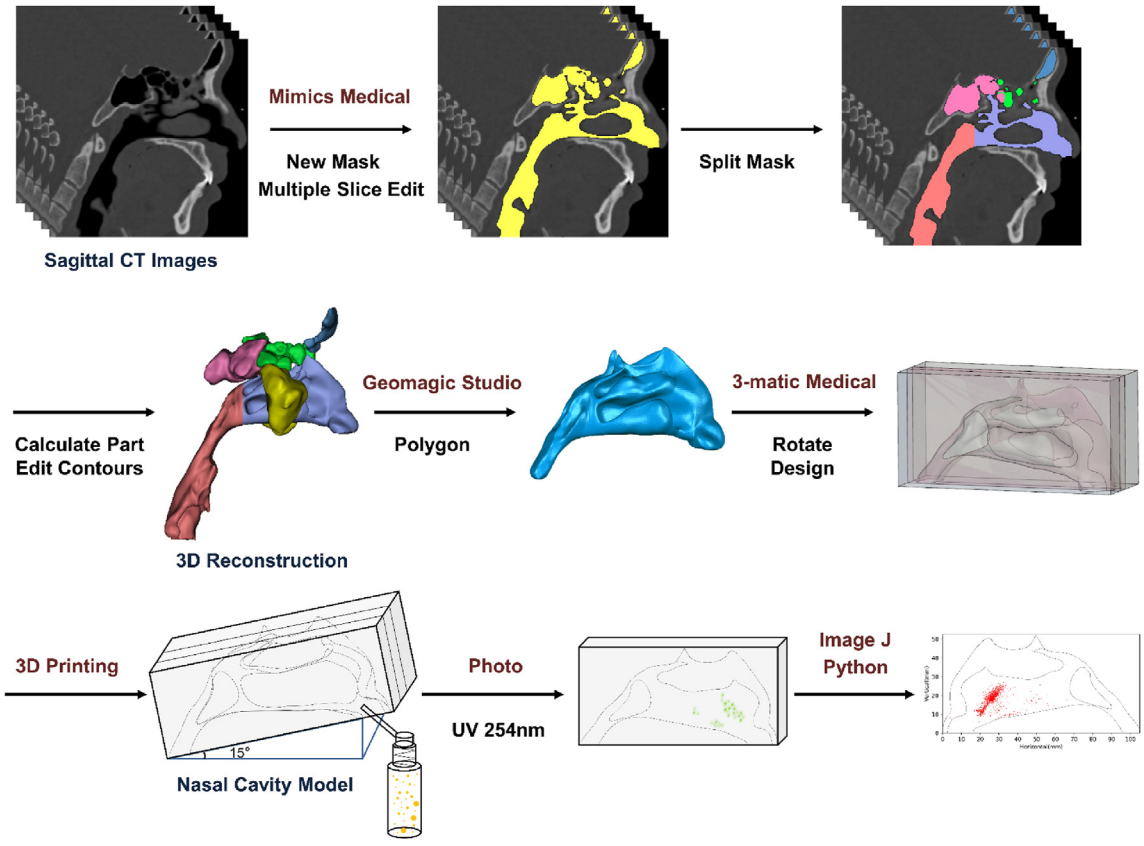


**Scheme 1** The 3D reconstruction of nasal cavity and evaluation of powder distribution.

for the two gender groups, which were thin enough to capture the characteristics of the nasal morphologies during the reconstruction of the three-dimensional (3D) nasal models. The freshly available heads of goats were procured at local food market, for which the head and neck CTs were acquired from Nantong Haimen People's Hospital.

The γ-cyclodextrin (γ-CD) was purchased from Maxdragon Biochem Co., Ltd. (Guangzhou, China). RhoB was acquired from Meryer Technologies Co., Ltd. (Shanghai, China). Dimethicone was purchased from Xinli Polymer Material Co., Ltd. (Dongguan, China). Potassium hydroxide (KOH), calcium chloride anhydrous ($CaCl_2$), sodium chloride (NaCl), potassium chloride (KCl), glycerol, methanol (MeOH), ethanol (EtOH), acetic acid, and polyethylene glycol 20,000 (PEG 20,000) of analytical grade and tris (hydroxymethyl) aminomethane of biochemical grade were obtained from Sinopharm Chemical Reagent Co., Ltd. (Shanghai, China). MF NS was purchased from Zhejiang Xianju Pharmaceutical Co., Ltd. (Taizhou, China). MF reference standard was purchased from National Institutes for Food and Drug Control (Beijing, China). Water was purified using a Master-s15UV laboratory water purification system (Hitech Instruments Co., Ltd., Shanghai, China).

### *2.2. 3D reconstruction of human nasal cavities and goat nasal cavities*

Mimics Medical (version 21.0, Materialise Nv, Belgium), 3D Slicer (National Institutes of Health, Boston, MA, USA), Simpleware (S-2021.06-SP1, Simpleware Ltd., Britain), and Amira (Visage Imaging Ltd., Australia) are the leading software used for the 3D reconstruction of medical images[30]. Mimics Medical software (Materialise Nv) was used to reconstruct the nasal cavity from the original CT scans in this study. A new mask was created to segment the nasal cavity. The external factors were then removed by region growth. A splitting mask was used to separate sinuses, and the nasal airway was preserved. After clearing the unclear areas of CT scanned images by multiple slice editing, the mask was calculated and smoothed to obtain the desired shape. The shape in STL + format was imported into Geomagic Studio software (version 2014 (64-bit), 3D Systems, USA). It was finely smoothed by filling a single hole and removing sharp edges. The above steps were repeated to reconstruct the nasal cavities of all subjects and goats.

### *2.3. Calculation of human nasal cavity structure parameters*

The most important structural parameters of the nasal cavity are the mucosal area, nasal volume, and the mucosal area-volume ratio. The nasal mucosal area, nasal volume, and nasal mucosal area-volume ratio of the fabricated nasal cavity were calculated to determine the differences between different ages and genders.

### *2.4. 3DP*

Before 3DP, the model was smoothed and cut with 3-matic Medical software (version 21.0, Materialise Nv, Belgium). There was a narrow passage between the nasal septum and the turbinate region, and the nasal cavity was cutting along the proper nasal passage in a sagittal plane. The human nasal cavity was divided into 3 regions using sagittal plane, namely the right parts including

turbinate and meatus region, the middle part including nasal septum region and the left part including left nasal cavity. The goat model was divided into 10 regions, consistent with real goat heads. 3DCST2500PLUS transparent resin (Shenzhen Qisiyin Technology Trading Co., Ltd., Shenzhen, China) was used to 3D print the right and middle parts and ordinary resin (Shenzhen Qisiyin Technology Trading Co., Ltd., Shenzhen, China) was used to 3D print the left part of the Chinese adult male and female nasal cavities. The reason why chose different materials for printing different parts was that the images of the powder distribution on the transparent resin were clearer than those on the ordinary resin, and the different materials also made it easier to distinguish the experimental objects from each other. UV curable translucent resin was used to make a goat nasal model (Nantong Haimen People's Hospital, Nantong, China). High-performance liquid chromatography (HPLC) was used for the quantitative analysis of drug deposition in goat nasal cavity model and the goat head, and it was not necessary to investigate the clarity of distribution of images, so this resin was selected.

### 2.5. Synthesis and characterization of nanoscale and microscale RhoB@MOFs

Metal-organic frameworks (MOFs) preparation method was adapted from a previously reported procedure[31,32]. Briefly, the molar ratio of γ-CD to KOH was 1: 8. γ-CD (12.96 g, 0.01 mol) and KOH (4.48 g, 0.08 mol) were dissolved in purified water (400 mL). The solution was filtered through an organic filter membrane (0.45 μm) in the case of nanoscale MOFs, whereas the microscale MOFs were synthesized without filtration. After adding methanol (240 mL), the rotating speed of the magnetic stirrer was set to 500 r/min (TDZ5-WS, Hunan Xiang Yi Laboratory Instrument Development Co., Ltd., Xiangyi, China) and stirred for 5 min. The reaction mixture was kept in a water bath (60 °C) until the solution was transparent and continued to react for 20 min after clarification. PEG20000 (2.56 g) was dissolved in anhydrous methanol (320 mL), and then this solution was added to the previously prepared mixture to synthesize nanoscale particles, while PEG20000 in solid form was added to synthesize microscale particles. Both of these mixtures were placed in a water bath (60 °C) with paddle stirring for 5 min. After stirring, it was incubated for 20 min in a water bath (60 °C), then transferred to a colder water bath and kept there for 2 h to precipitate crystals. The precipitates were collected by centrifugation, washed with ethanol and methanol, and dried at 70 °C for 3 h to obtain white powders of cubic crystal particles. CD-MOFs (1.5 g) of nano-size or micron-size and RhoB (0.5 g) were suspended/dissolved in methanol (50 mL). After magnetic stirring for 1 h, precipitates were obtained by centrifugation. The RhoB@MOFs of nano-size or micron-size were obtained after drying the precipitates for 3 h.

The surface morphology and size of the nanoscale CD-MOFs, microscale CD-MOFs, nanoscale RhoB@MOFs and microscale RhoB@MOFs were observed under scanning electron microscopy (SEM; JSM-IT500HR/LA, JEOL Ltd., Japan) operated at a beam voltage of 10 kV.

### 2.6. Image acquisition and processing

In this study, RhoB@MOFs were used as the standard nasal powder due to its fluorescence effect. The powder (3 g) was dried at 70 °C before use and was loaded into a drug delivery device. The device was used to measure the distribution pattern of powder by spraying it. The nasal cavity model was placed under a 254 nm UV analyzer (WFH-203B, Hangzhou Qiwei Technology Co., Ltd., China) because RhoB@MOFs exhibited orange fluorescence at a wavelength of 254 nm. The photos were taken at a fixed camera location by placing the nasal cavity model on an inclined plane with a slope of 10° to obtain a parallel image to the lens. The photosensitivity was set to 1600 and the shutter speed to 2 s in the original model to ensure the consistency of the photo parameters. The photos were imported into ImageJ software (version 1.53t, National Institutes of Health, America) and cropped. After adjusting brightness and contrast, the color selection threshold was used to extract powder distribution. The extraction of the nasal profile was combined with the extraction of powder distribution. Python (version 3.6, Python Software Foundation, USA) was applied to process the images to get the final images with coordinates. The images were divided into several regions according to the physiological structure of the nasal cavity, and the distribution area of the regions was measured respectively to calculate the percentage.

### 2.7. Comparison of the deposition pattern in human nasal models

In this study, an appropriate solution for preventing the entrainment phenomenon and simulating the nasal environment was examined and selected. The deposition patterns at different spraying times, particle sizes, administration angles, and genders were then investigated. Dry powder spray devices were used to simulate drug delivery. Distribution images were captured and processed according to Section 2.6.

#### 2.7.1. Coating solutions

The nasal cavity models were assembled with every surface lined with dimethicone, artificial mucus 1, artificial mucus 2, and uncoated surfaces, respectively. Artificial mucus 1 was composed of a 75:25 ethanol: glycerol mixture[33]. Artificial mucus 2 was composed of 8.761 g NaCl, 2.982 g KCl, 0.555 g $CaCl_2$ and 1.211 g Tris. The volume of the solution was fixed to 1 L, and the pH was adjusted to 6.3 after being dissolved in deionized water. Nanoscale RhoB@MOFs powders were injected at a depth of 10 mm into the nostrils at an angle of 30° to the horizontal. In this section, only nanoscale RhoB@MOFs were used to investigate the coating solution. The distribution of RhoB@MOFs in nasal cavity model with different particle sizes will be discussed in Section 2.7.3.

#### 2.7.2. Spraying times

The deposition pattern was assessed by uniformly coating the transparent nasal cavity model with dimethicone. The dry powder device tip was inserted 10 mm into the nostril at an administration angle of 30° to the horizontal and sprayed 1, 5, and 10 times, respectively.

#### 2.7.3. Particle sizes

The nanoscale and microscale powders were filled into the drug delivery device. Dry powder preparation was applied at a 45° angle from the horizontal at a nostril insertion depth of 10 mm and sprayed five times.

#### 2.7.4. Administration angles

Dry powder preparation was injected into the dimethicone-coated nose model at an angle of 30°, 45°, and 60° to the horizontal and at

a tip insertion depth of 10 mm. The parameters optimized during the above experimental steps were selected under other conditions.

#### 2.7.5. Genders

Dimethicone-coated male and female nasal cavity models were tested with a 45° administration angle and insertion depth of 10 mm, and spraying 5 times, respectively.

### 2.8. Segmentation methods

One segmentation method used was to slice the nasal cavity along the meatus nasi communis in a sagittal plane to separate the nasal septum and nasal concha region. Another method used was to slice the nasal cavity in a coronal plane based on the midpoint of the line between the anterior naris and posterior naris, divided into the anterior part of the nasal cavity and the posterior part of the nasal cavity, so as to try the powder distribution effect from different perspectives. The other experimental conditions were the same as before.

### 2.9. Methodology feasibility verification

#### 2.9.1. Determination of mometasone furoate in model and in goat

MF distributed on the surface of the model was determined using an Agilent 1290 infinity (Agilent 1290, Agilent Technologies, Inc., Palo Alto, CA, USA) with photo-diode-array-detector (DAD, G4212A). Chromatographic column was InerSustain AQ-C18 (250 mm × 4.6 mm, 5 μm). MF was detected at 254 nm with column temperature of 40 °C and a flow rate of 1.0 mL/min. The mobile phase consisted of methanol (A) and 0.2% acetic acid in water (B) (75:25, *v*/*v*).

MF in goat cavity was also analyzed using the same HPLC system. However, in order to eliminate the interference of impurities in biological samples, the proportion of the mobile phase was optimized to gradient conditions as follows: mobile phase B was maintained at 70% (*v*/*v*) from 0 to 18 min, decreased from 70 to 10% (*v*/*v*) for 18−19 min, maintained at 10% (*v*/*v*) from 19 to 22 min, increased from 10% to 70% for 22−23 min, and maintained at 70% from 23 to 25 min. The other chromatographic conditions were the same as in the *in vitro* test.

#### 2.9.2. Distribution of nasal deposition in goat nasal cavity

Each goat nose was divided into 5 parts from front to back with each area about 2 cm wide. And then each area was divided into 2 parts along the nasal septum. Anatomically, the nasal turbinate region and the nasal septum were divided into five regions respectively, 10 regions in total for each nasal cavity (Fig. 1). MF NS was used as the standard preparation, for which the insertion depth was about 10 mm, the spray angle was set as 45°, and the spray time was 5. The nasal cavity was cut along the nasal septum, the mucosa was peeled off for each part. The mucosa was placed in about 1 mL anhydrous methanol and vortexed for 30 s, and the washing liquid was transferred to the centrifuge tube. The washing process was repeated 5 times. The washing liquid was mixed and centrifuged at 4000 r/min (TDZ5-WS, Hunan Xiang Yi Laboratory Instrument Development Co., Ltd., Xiangyi, China) for 5 min, and then the supernatant was dried with nitrogen at 40 °C. The residue was added with 1 mL methanol for redissolution, swirled for 1 min, centrifuged for 5 min at 12,000 r/min (1730R, Shanghai Baygene Biotechnologies Co., Ltd., Shanghai, China) and the supernatant was taken for sample analysis according to Section 2.9.1.

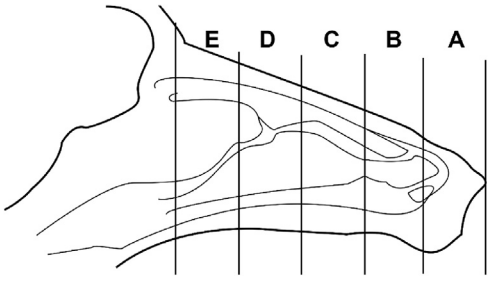


**Figure 1** Segmentation of the goat nasal cavity.

#### 2.9.3. Distribution of nasal deposition in goat nasal cavity model

The nasal cavity model of goat was sealed and fixed with rubber bands. MF NS was used as the standard preparation and sprayed for 5 times. The model was disassembled and rinsed with about 1 mL of anhydrous methanol and repeated washing 5 times. The washing solution was collected. The washing solution was combined and dried with nitrogen at 40 °C. The residue was added with 1 mL of methanol for resolution, vortexed for 1 min, centrifuged for 5 min at 12,000 r/min (Shanghai Baygene Biotechnologies Co., Ltd.), and the supernatant was taken for sample analysis according to Section 2.9.1.

## 3. Results and discussion

### 3.1. 3D reconstruction model

The nasal structures were reconstructed by Mimics software (Materialise Nv). The nasal and pharyngeal regions of a 40-year-old male were anatomically selected from coronal, sagittal, and axial CT images (Fig. 2A). The relative positions of the sinuses, including the frontal sinus, ethmoid sinus, maxillary sinus, and sphenoid sinus, with respect to the nasal cavity and nasopharynx, were shown from different sides (Fig. 2B). The nasal cavity and pharynx were separated by the posterior nostril (Fig. 2C). The sinuses and nasal cavity regions of a male goat were clearly visible through reconstruction (Fig. 2D).

### 3.2. 3D reconstruction model analysis

The ratio of nasal mucosal surface area to nasal volume is considered a reliable, accurate, and effective index for measuring the degree of airway stenosis. Due to the fact that this index is a ratio, its value is less affected by differences in the physiques of patients[34]. In this study, the nasal cavities of 16 male and 16 female Chinese adults were reconstructed, with ages ranging from 20 to 59. The spatial distribution relationship of the nasal cavity area, volume and area to volume ratio between males and females was determined by age (Fig. 3A−C). The nasal mucosal area and nasal volume showed low age correlation but significant gender differences, which indicated that the age of adults did not change nasal cavity structures (Table 1). The area and volume of nasal mucosa in males were generally larger than those in females, and the ratio was lower (Table 2). The area and volume between the genders were statistically significant, but the ratio was not different. Zang et al.[35] concluded that gender had no significant

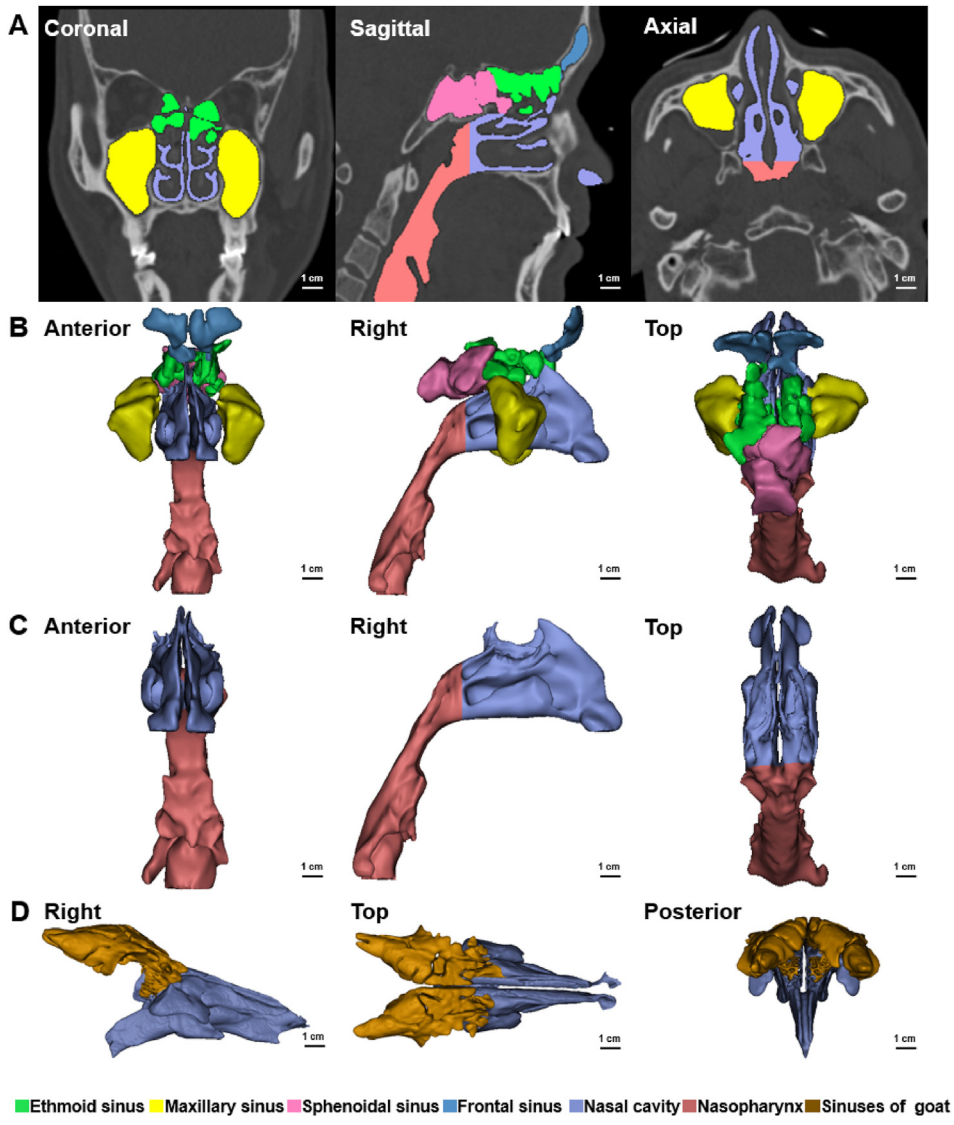


**Figure 2** The 3D reconstruction digital human and goat models. (A) 3D reconstruction of male human nasal cavity in CTs; (B) 3D reconstruction of nasal and pharyngeal regions in male human; (C) 3D reconstruction of nasal cavity and pharynx in male human; (D) 3D reconstruction of nasal and pharyngeal regions in male goat.

impact, which differed from the study in this paper. Experimental data showed the need for a single-factor experiment that targeted gender-related physiological differences.

### *3.3. 3DP evaluation model and blank model processing*

Previously, the average area and volume of the male and female nasal cavities were analyzed, and the one closest to the average area and volume of the male and the one closest to the average female nasal cavity were selected respectively in 3DP. 3-Matic Medical software (Materialise Nv) was used to design the evaluation models (Fig. 4A, C and E). After submitting the standard triangle language (STL) format and selecting the corresponding materials for printing, the biomimetic nasal cavity models were obtained. They had good complete resemblance to the nasal cavity structure and could be used to determine the deposition pattern of drugs within the nose (Fig. 4B, D and F). Two different gender resin nasal casts were used for the following experiments. The blank male nasal cavity model was extracted with a wire frame, and the corresponding physiological structure was marked (Fig. 5A and B). The anatomy of the nasal cavity was drawn to facilitate a better understanding of the physiological structure corresponding to the wireframing diagram (Fig. 5C). In order to facilitate the calculation of deposition areas in subsequent experiments, the model was divided into eight regions according to the nasal anatomy: a) anterior nasal vestibule; b) posterior nasal vestibule; c) anterior nasal septum; d) posterior nasal septum; e) anterior inferior nasal concha; f) middle of inferior nasal concha; g) posterior inferior nasal concha; and h) inferior nasal meatus (Fig. 5D and E).

### *3.4. Nasal powder deposition in nasal cavity model*

#### *3.4.1. Coating solutions*

In order to prevent the entrainment phenomenon caused by particle rebound during the test, which may cause loss and distribution measurement error and affect the experimental results, it is necessary to select a suitable coating solution for the device to

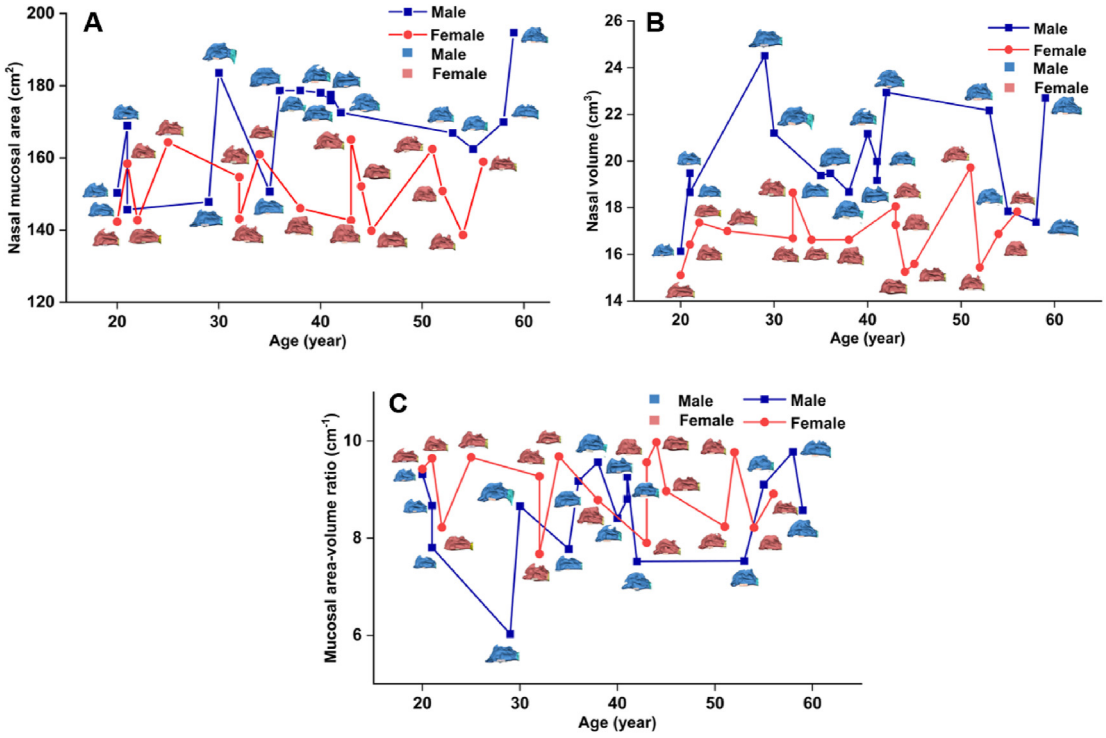


**Figure 3** Distribution of human nasal cavity with age. (A) Distribution chart of the human nasal mucosal area with age; (B) Distribution chart of the human nasal volume with age; (C) Distribution chart of the human nasal mucosal area-volume ratio with age.

**Table 1** Comparison of nasal mucosal area, nasal volume, and mucosal area-volume ratio distribution in different age groups.

| Age group (year) | *n* | Average nasal mucosal area ($cm^2$) | Average nasal volume ($cm^3$) | Average mucosa area-volume ratio ($cm^{-1}$) |
|---|---|---|---|---|
| [20, 30) | 8 | 152.56 ± 10.12 | 18.09 ± 2.95 | 8.60 ± 1.24 |
| [30, 40) | 8 | 162.05 ± 16.01 | 18.41 ± 1.66 | 8.82 ± 0.76 |
| [40, 50) | 8 | 162.96 ± 15.90 | 18.68 ± 2.67 | 8.80 ± 0.83 |
| [50, 60) | 8 | 163.10 ± 16.16 | 18.75 ± 2.57 | 8.76 ± 0.79 |
| [20, 60) | 32 | 160.17 ± 14.76 | 18.48 ± 2.40 | 8.75 ± 0.88 |

Data are shown as mean ± SD.

**Table 2** Comparison of nasal mucosal area, nasal volume, and mucosal area-volume ratio distribution in different genders.

| Gender | Average nasal mucosal area ($cm^2$) | Average nasal volume ($cm^3$) | Average mucosal area-volume ratio ($cm^{-1}$) |
|---|---|---|---|
| Male | 168.90 ± 14.15 | 20.06 ± 2.24 | 8.50 ± 0.97 |
| Female | 151.44 ± 9.35*** | 16.91 ± 1.26*** | 8.99 ± 0.74 |
| *P* value | 0.00028 | 0.000031 | 0.11 |

Data are presented as mean ± SD ($n = 16$). ***$P < 0.001$, *versus* Male.

simulate the moist environment of the nasal cavity[36]. The results showed that the deposition area was higher in the posterior nasal septum and posterior inferior nasal concha for both blank and artificial mucus, and part of the powder fell into the nasopharynx (Fig. 6A). In the blank model, the posterior model distribution percentage was 87.72 ± 3.50% due to the entrainment effect. Moreover, 61.97 ± 3.66% of artificial mucus 1 and 68.04 ± 10.63% of artificial mucus 2 showed no significant improvement in the phenomenon (Fig. 6B). Since the transparent resin was a hydrophobic material, two artificial mucus used tended to form droplets of varying sizes on the surface of the device[37]. The powder that was soluble in water entered the nasal cavity model, so it was easy to dissolve in the artificial mucus, resulting in the current distribution image[38]. However, most of the powders were deposited *in situ*, and 29.07 ± 7.38% of the powder in the posterior model significantly reduced backward deposition in the pharynx when coated with dimethicone. Dimethicone can be evenly coated onto the surface of the device, and the powder did not dissolve and diffuse when contacted with dimethicone. Thus, dimethicone was a suitable material for measuring powder deposition, and it was selected for use as a coating solution compatible with the test device.

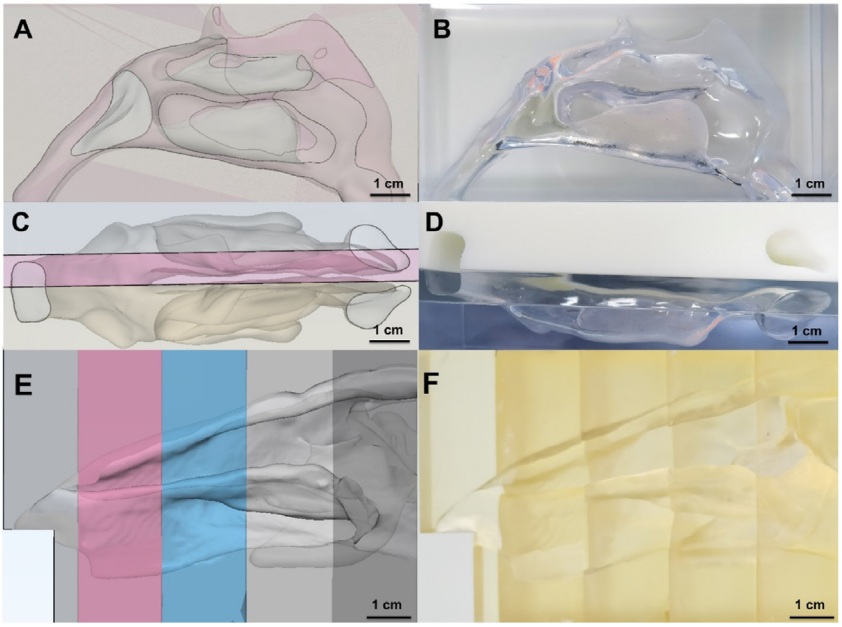


**Figure 4** Human and goat nasal cavity model. (A) Right view of the design of human models; (B) Right view of human devices (C) Bottom view of the design of human models; (D) Bottom view of human devices; (E) Left view of the design of goat models; (F) Left view of goat devices.

*3.4.2. Spray times*

In order to better observe the fluorescence distribution of powder, the investigation of spraying times was extremely important. The shortcomings of uneven dose of the device would be obviously exposed at 1 spray, such as the anterior nasal septum was 41.77 ± 28.95%, and intermediate inferior nasal concha was 46.67 ± 24.28% (Fig. 7A and B). There was no significant difference in the distribution data between the 5 and 10 sprays, 55.60 ± 4.30% and 51.20 ± 7.03% in the anterior nasal septum, respectively. It was obvious that spraying 5 times reduced device error and allowed a clear view of powder distribution. Although the distribution of 10 times was not much different from that of five times, it seemed sufficient to use 5 times.

*3.4.3. Particle sizes*

The particle sizes of powders will affect the site of nasal deposition and the use of drug delivery devices[39]. The deposition distribution of different particle sizes of powders in the nasal cavity model demonstrated that the current use of drug delivery devices simply cannot spray microscale powder as indicated by

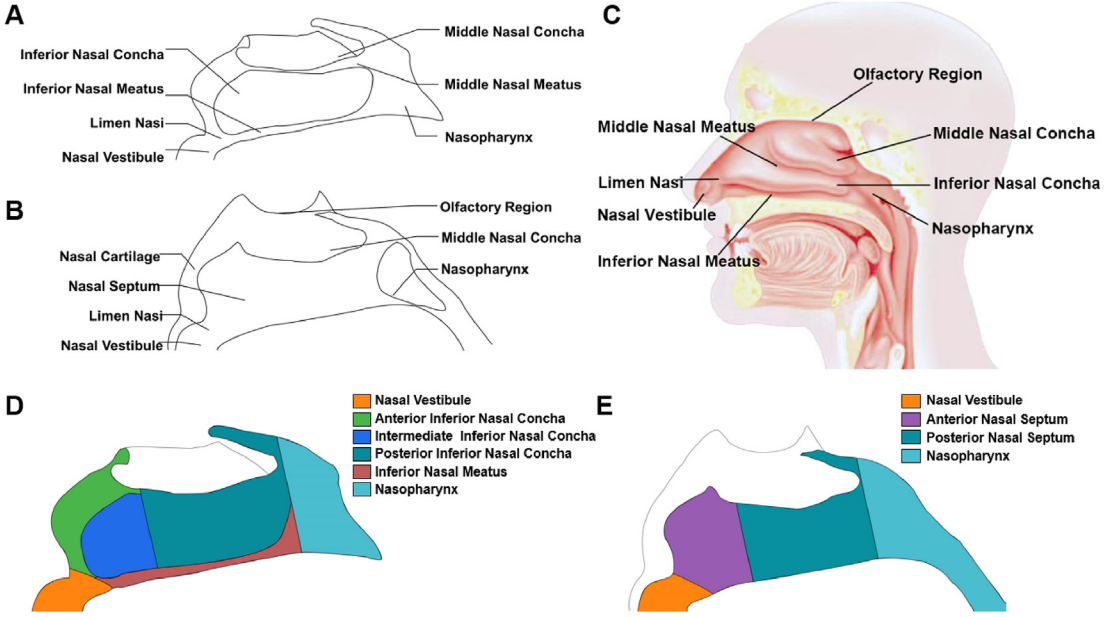


**Figure 5** Nasal structure and physiological structure division. (A) Schematic diagram of the nasal cavity in the right model; (B) Schematic diagram of the nasal cavity in the middle model; (C) Nasal anatomy diagram; (D) Division of the nasal cavity in the right model; (E) Division of the nasal cavity in the middle model.

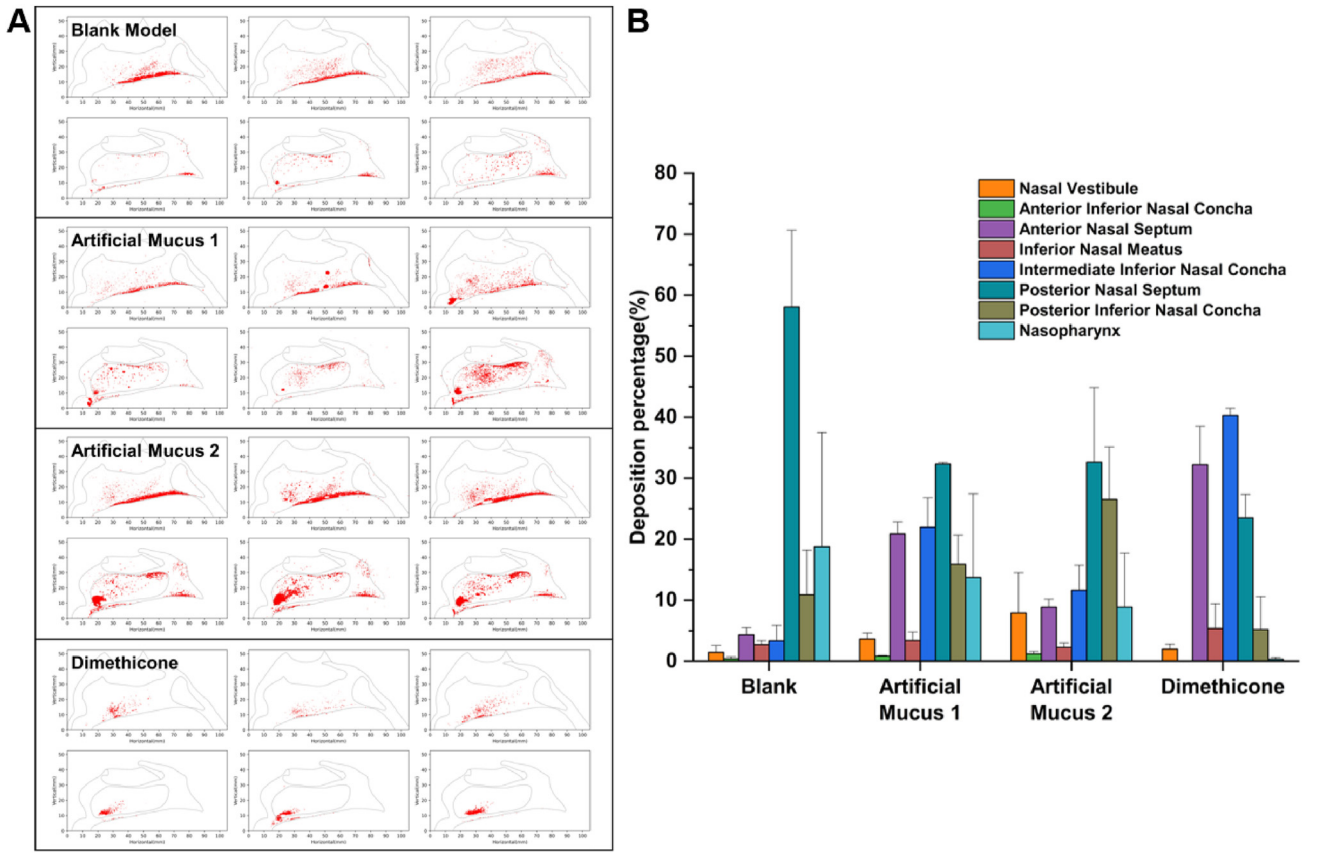


**Figure 6** Powder distribution of different coating solutions in nasal cavity model. (A) Powder distribution; (B) Deposition percentage in different areas of the nasal cavity.

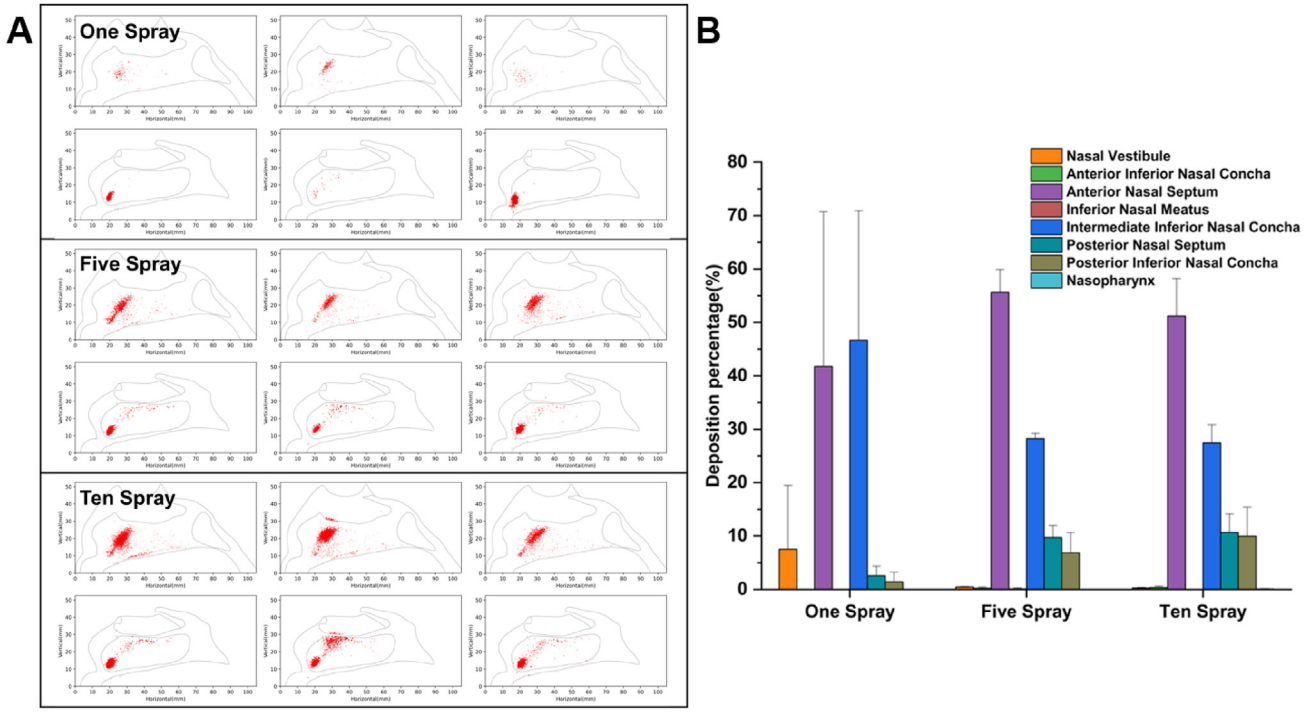


**Figure 7** Powder distribution of different spray times in nasal cavity model. (A) Powder distribution; (B) Deposition percentage in different areas of the nasal cavity.

the distribution in the nasal cavity model (Fig. 8B and C). CD-MOFs had a cubic structure, and the size distribution of nanoscale CD-MOFs were mainly 200−300 nm, whilst the size distribution of microscale CD-MOFs were mainly 1−3 μm. After physical staining with RhoB, RhoB@CD-MOFs still presented a good cubic appearance structure and the size distribution of nanoscale RhoB@MOFs remained about 200−300 nm, whilst size of microscale RhoB@MOFs remained about 1−3 μm (Fig. 8A). The particle size investigation showed that the particle size range suitable for the nozzle of the device had a good distribution below a micron. This experiment showed the capability of the biomimetic nasal cavity model to indicate the compatibility between the device and the powder, especially for powder formulation optimization.

### 3.4.4. *Spray angles*

The spray angles had a significant influence on the height and depth that the powder could reach[26]. When the injection angle was 30°, the powders mainly deposited in the intermediate inferior nasal concha, accounting for 40.30 ± 1.16%, and 5.39 ± 4.05% deposited in the inferior nasal meatus (Fig. 9A and B). In contrast, 53.42 ± 4.30% powder in the anterior nasal septum with a 45° spray angle and 46.87 ± 11.41% in the anterior inferior nasal concha with a 60° spray angle. Incidence angles had obvious effects on distributions. For the treatment of disease, the location of the lesion can be identified through CT examination or nasal endoscopy to guide the selection of spray angles to send most drugs to the effective site. For the treatment of inferior nasal meatus, the device should be positioned at a horizontal angle of 30° then sprayed, while for treating

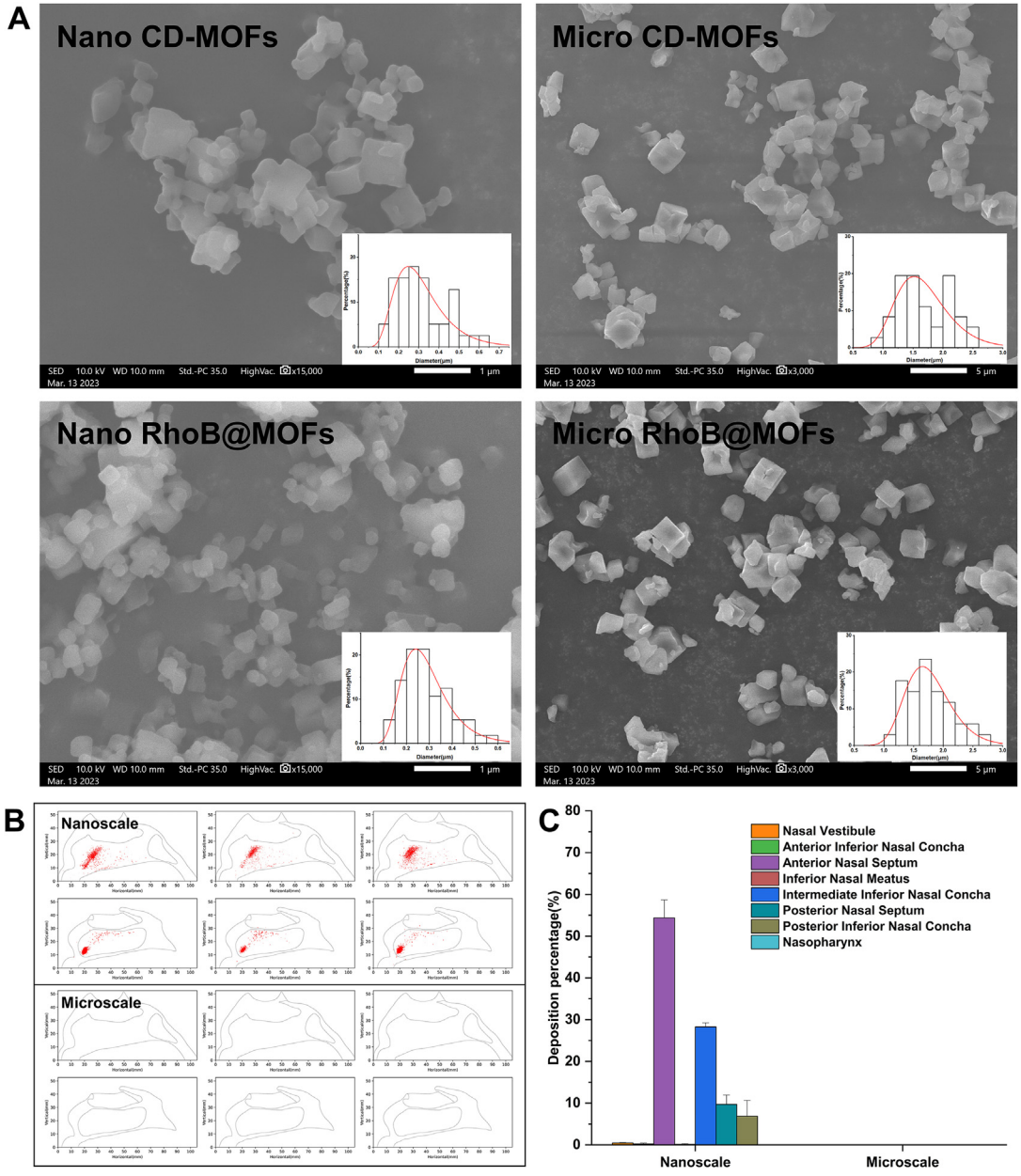


**Figure 8** SEM images of nanoscale CD-MOFs, microscale CD-MOFs, nanoscale RhoB@MOFs and microscale RhoB@MOFs and powder distribution of different particle sizes in nasal cavity model. (A) SEM images of nanoscale powders (scale bar = 1 μm) and microscale powders (scale bar = 5 μm); (B) Powder distribution; (C) Deposition percentages in different areas of the nasal cavity.

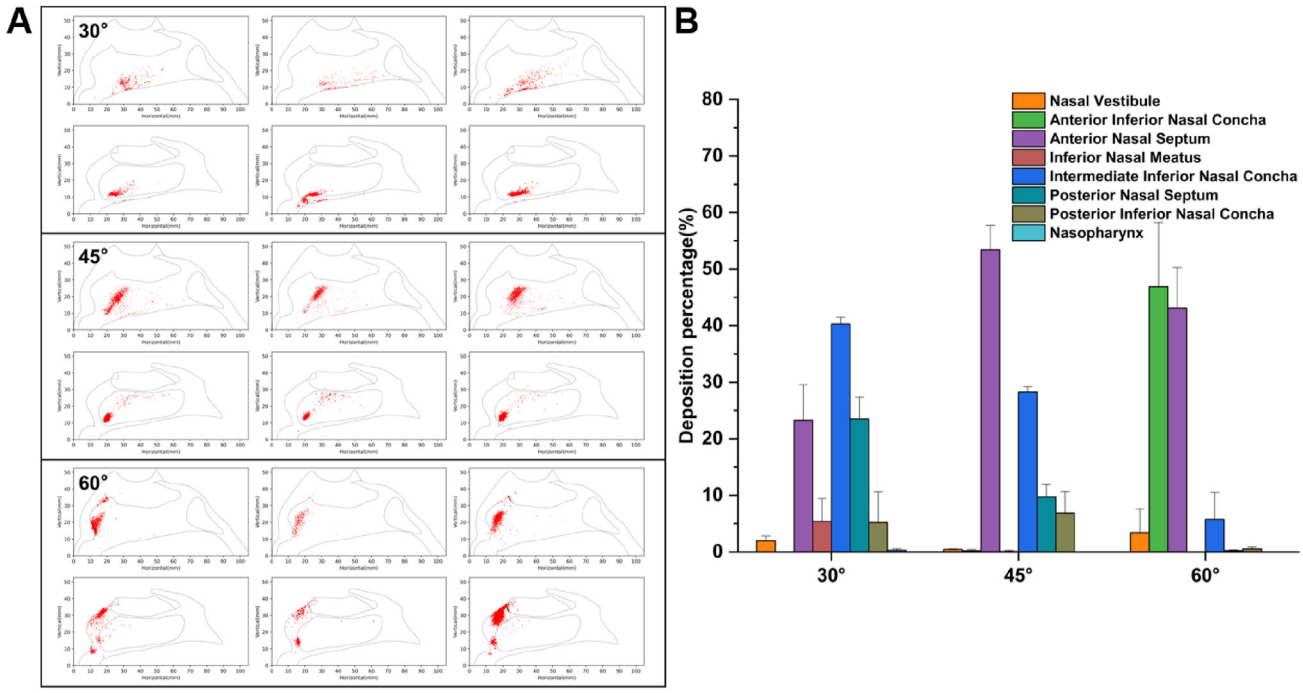


**Figure 9** Powder distribution of different spray angles in nasal cavity model. (A) Powder distribution; (B) Deposition percentage in different areas of the nasal cavity.

central nervous diseases, the incidence angle should be about 60°. The investigation of spray angles was of great importance in guiding the personalized use of nasal spray drugs.

### *3.4.5. Genders*

There were significant differences in nasal cavity area and volume between different genders. At present, there are few studies on nasal drug sedimentary distribution for gender. At the same spray angle, the distribution of powders in the female nasal cavity was more concentrated at a depth of 10−30 mm, and the deposition percentage was 96.27 ± 2.69%, while it was more dispersed in the male nasal cavity at a depth of 20−70 mm and 65.59 ± 7.07% powder in the anterior nasal cavity (Fig. 10A and B). Although there was no significant difference in the area-volume ratio between males and females, the distribution difference was highly varied. It was speculated that the reason for this phenomenon was that the front end of the inferior nasal meatus and the nasal septum of the females was narrower than that of the males, and the powder was easy to distribute in the frontal nasal cavity of females.

### *3.5. Segmentation methods*

In order to observe the powder deposition in the nasal cavity from different perspectives, two slicing methods were evaluated. One way was to slice the nasal cavity in a coronal plane based on the midpoint of the line between anterior naris and posterior naris (Fig. 11A). The other way was to slice the nasal cavity along

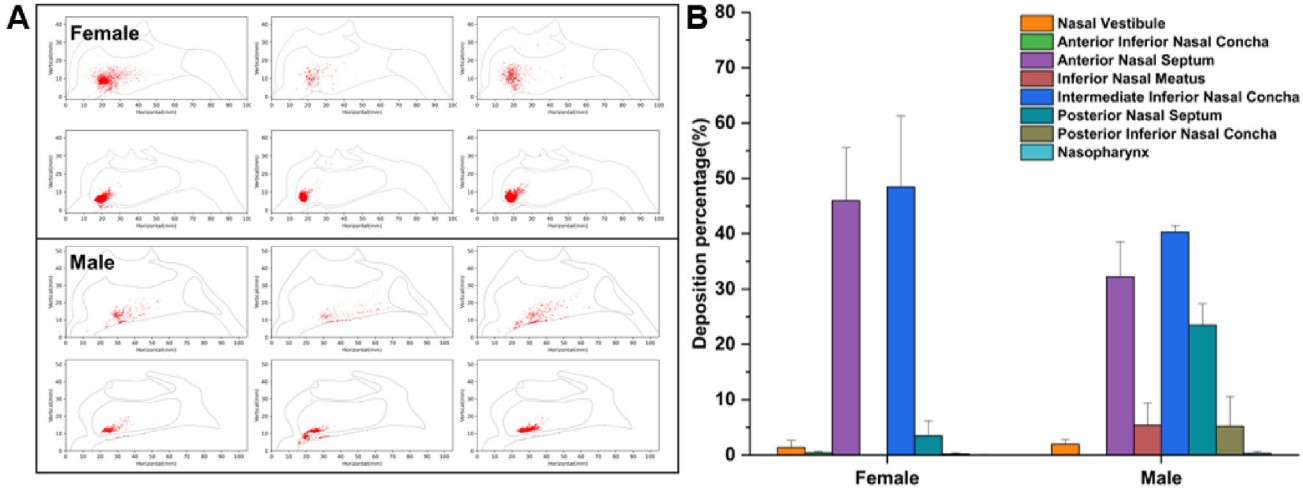


**Figure 10** Powder distribution of different genders in nasal cavity model. (A) Powder distribution; (B) Deposition percentage in different areas of the nasal cavity.

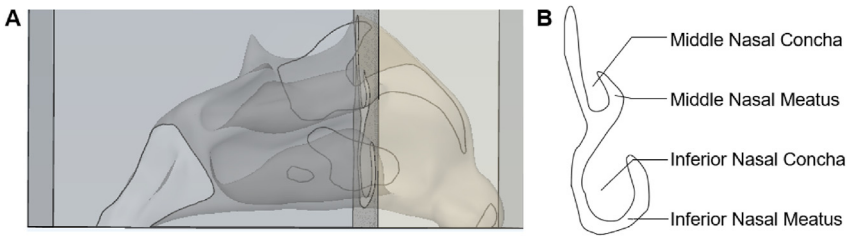


**Figure 11** Schematic diagram of nasal cavity model cutting and physical wireframe extraction. (A) A schematic diagram of nasal cavity model cutting; (B) Physical wireframe extraction.

meatus nasi communis in a sagittal plane to separate nasal septum and nasal concha region (Fig. 4A and C). It was evident that the extracted wire frame in a coronal plane showed less structure information than the sagittal plane slice, and the distribution of the nasal septum and other positions cannot be clearly observed (Fig. 11B). Moreover, the powder deposition in the hollow nasal cavity made it impossible to take a good distribution map. Therefore, the sagittal plane slice way was selected and better demonstrated the powder distribution.

### 3.6. *Methodology feasibility verification*

The *in vivo* accumulated depositions were compared with the *in vitro* accumulated depositions for the same spray method, and a quantitative correlationship was established using linear regression. The results showed that MF NS had good linear correlation between *in vitro* and *in vivo* with $R^2$ of 0.9657 in nasal septum, 0.9823 in nasal turbinate, and 0.9860 in total, respectively (Fig. 12).

It was interesting to note that some special issues were experienced during the experiment. First of all, the nasal cavity model of a goat was made of rigid resin, which wasn't similar in elasticity to the goat's nose mucosa. The model couldn't completely cover the nozzle, which allowed some drugs to escape into the air, resulting in drug quantity loss in zone A, and the total amount of zone A and zone B was less than that in the goat's nasal cavity. Secondly, the surface of the goat's nose was covered with nasal fluid and vomit, which was different from the case of the model. Moreover, it was difficult to accurately divide goat nose regions as the models were, which might introduce some experimental errors.

Despite these challenges, the distributions of MF NS were very similar in the goat nasal cavity and in the 3D printed goat nasal cavity model with good *in vitro* and *in vivo* correlation demonstrating the feasibility of the nasal model for evaluating the distribution of nasal preparations. Compared with goat nose, the model was more convenient and reproducible in operation and measurement.

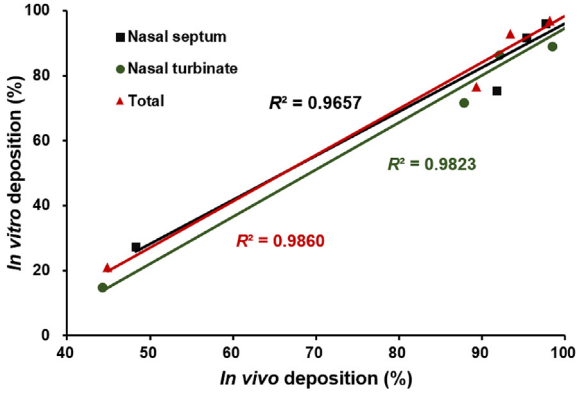


**Figure 12** The *in vitro* and *in vivo* correlations of accumulated MF deposition in the nasal cavity.

## 4. Conclusions

In summary, 3D reconstruction and 3DP technology provided a useful framework for establishing a biomimetic nasal cavity model for nasal powdered spray drug evaluation and personalized therapeutic guidance. The reconstruction process revealed that the area and volume of human nasal cavity structure were significantly different between Chinese males and females, while the age of adults does not change nasal cavity structures. Interestingly, the powders were inclined to deposit at the front of the nasal cavity in females but tended to deposit at the posterior nasal cavity in males. The biomimetic nasal cavity evaluation device printed with transparent resin in combination with dimethicone coating can successfully simulate the human physiological nasal cavity, and spray times should be optimized for quality control of the nasal spray dosage form. Spray angles have a significant impact on powder deposition/distribution. In the case of nasal delivery for nose-to-brain delivery, an angle of 60° could be used to send powders to the olfactory region. The male goat nasal cavity model with good *in vitro and in vivo* correlation demonstrated the feasibility of the nasal model for evaluating the distribution of nasal preparations. Compared with goat noses, the 3D printed model was more convenient and reproducible in operation and measurement. In conclusion, the human nasal structure biomimetic device has been shown to be efficient in evaluating the deposition/distribution of nasal drug delivery systems.

## Acknowledgments

This research was funded by the Key Program for International Science and Technology Cooperation Projects of China (No. 2020YFE0201700), the Innovation Leading Talents Short-term Program of Jiangxi Province, China (No. 1262000102), and Shanghai Science and Technology Plan (No. 21DZ2260400, China).

## Author contributions

Li Wu, Rui Yang, Zhigang Wang, and Jiwen Zhang designed the research. Jiawen Su, Yan Liu, and Yue Qu carried out the experiments and performed data analysis. Hongyu Sun, and Huipeng Xu processed images and data. Abid Naeem, Jie Wu, Lixin Sun, Lulu

Wang, and Xiaofeng Wang provided suggestions on the standardization of experiments. Caifen Wang, Zeru Li and Jianhua Lu contributed to the experimental work for revision and supplemented tests. All the co-authors wrote and revised the manuscript. All of the authors have read and approved the final manuscript.

## Conflicts of interest

The authors have no conflicts of interest to declare.

## References


1. Laffleur F, Bauer B. Progress in nasal drug delivery systems. *Int J Pharm* 2021;**607**:17.
2. Appasaheb PS, Manohar SD, Bhanudas SR. A review on intranasal drug delivery system. *J Adv Pharm Educ Res* 2013;**3**:333. 46.
3. Cunha S, Amaral MH, Lobo JMS, Silva AC. Lipid nanoparticles for nasal/intranasal drug delivery. *Crit Rev Ther Drug Carrier Syst* 2017;**34**:257. 82.
4. Varshosaz J, Sadrai H, Heidari A. Nasal delivery of insulin using bioadhesive chitosan gels. *Drug Deliv* 2006;**13**:31. 8.
5. Costantino HR, Illum L, Brandt G, Johnson PH, Quay SC. Intranasal delivery: physicochemical and therapeutic aspects. *Int J Pharm* 2007;**337**:1−24.
6. Illum L. Nasal drug delivery: new developments and strategies. *Drug Discov Today* 2002;**7**:1184. 9.
7. Thomann-Harwood L, Kaeuper P, Rossi N, Milona P, Herrmann B, McCullough K. Nanogel vaccines targeting dendritic cells: contributions of the surface decoration and vaccine cargo on cell targeting and activation. *J Control Release* 2013;**166**:95−105.
8. Bahamondez-Canas TF, Cui ZR. Intranasal immunization with dry powder vaccines. *Eur J Pharm Biopharm* 2018;**122**:167. 75.
9. Van Woensel M, et al. Formulations for intranasal delivery of pharmacological agents to combat brain disease: a new opportunity to tackle GBM?. *Cancers* 2013;**5**:1020. 48.
10. Costa C, Moreira JN, Amaral MH, Sousa Lobo JM, Silva AC. Nose-to-brain delivery of lipid-based nanosystems for epileptic seizures and anxiety crisis. *J Control Release* 2019;**295**:187−200.
11. Costa C, Moreira J, Lobo JS, Silva A. Intranasal delivery of nanostructured lipid carriers, solid lipid nanoparticles and nanoemulsions: a current overview of *in vivo* studies. *Acta Pharm Sin B* 2021;**11**:925. 40.
12. Martin V, Hoekman J, Aurora SK, Shrewsbury SB. Nasal delivery of acute medications for migraine: the upper *versus* lower nasal space. *J Clin Med* 2021;**10**:2468.
13. Bi CC, et al. Intranasal delivery of rotigotine to the brain with lactoferrin-modified PEG-PLGA nanoparticles for Parkinson's disease treatment. *Int J Nanomed* 2016;**11**:6547. 59.
14. Meng QQ, et al. Intranasal delivery of Huperzine A to the brain using lactoferrin-conjugated *N*-trimethylated chitosan surface-modified PLGA nanoparticles for treatment of Alzheimer's disease. *Int J Nanomed* 2018;**13**:705. 18.
15. Yan XJ, et al. Lactoferrin-modified rotigotine nanoparticles for enhanced nose-to-brain delivery: LESA-MS/MS-based drug biodistribution, pharmacodynamics, and neuroprotective effects. *Int J Nanomed* 2018;**13**:273. 81.
16. Alagusundaram M, Chengaiah B, Gnanaprakash K, Ramkanth S, Chetty CM, Dhachinamoorthi D. Nasal drug delivery system-an overview. *Int J Res Pharm Sci* 2010;**1**:454. 65.
17. Ghori MU, Mahdi MH, Smith AM, Conway BR. Nasal drug delivery systems: an overview. *J Clin Endocrinol Metab* 2015;**96**:2997−3006.
18. Chen J, Wang XM, Wang J, Liu GL, Tang X. Evaluation of brain-targeting for the nasal delivery of ergoloid mesylate by the microdialysis method in rats. *Eur J Pharm Biopharm* 2008;**68**:694−700.
19. Pardeshi CV, Rajput PV, Belgamwar VS, Tekade AR. Formulation, optimization and evaluation of spray-dried mucoadhesive microspheres as intranasal carriers for Valsartan. *J Microencapsul* 2012;**29**:103. 14.
20. Scherlie R. Nasal formulations for drug administration and characterization of nasal preparations in drug delivery. *Ther Deliv* 2020;**11**:5−9.
21. Illum L. Nasal drug delivery—recent developments and future prospects. *J Control Release* 2012;**161**:254. 63.
22. Salade L, Wauthoz N, Goole J, Amighi K. How to characterize a nasal product. The state of the art of *in-vitro* and *ex-vivo* specific methods. *Int J Pharm* 2019;**561**:47−65.
23. Djupesland PG. Nasal drug delivery devices: characteristics and performance in a clinical perspective—a review. *Drug Delivery Transl Res* 2013;**3**:42−62.
24. Mayank C. A review on mucoadhesive polymer used in nasal drug delivery system. *J Adv Pharm Technol Res* 2011;**2**:215. 22.
25. Kundoor V, Dalby RN. Assessment of nasal spray deposition pattern in a silicone human nose model using a color-based method. *Pharm Res (N Y)* 2010;**27**:30.
26. Kundoor V, Dalby RN. Effect of formulation- and administration-related variables on deposition pattern of nasal spray pumps evaluated using a nasal cast. *Pharm Res (N Y)* 2011;**28**:1895. 904.
27. Lungare S, Bowen J, Badhan R. Development and evaluation of a novel intranasal spray for the delivery of amantadine. *J Pharmaceut Sci* 2016;**105**:1209. 20.
28. Hu XX, et al. Nanoporous CD-MOF particles with uniform and inhalable size for pulmonary delivery of budesonide. *Int J Pharm* 2019;**564**:153. 61.
29. Li H, et al. Paeonol loaded cyclodextrin metal-organic framework particles for treatment of acute lung injury *via* inhalation. *Int J Pharm* 2020;**587**:119649.
30. Fang WY, Lin DX. Advances in medical image three-dimensional reconstruction system. *Chin J Med Phys* 2022;**39**:823. 7.
31. Liu BT, et al. Optimized synthesis and crystalline stability of γ-cyclodextrin metal-organic frameworks for drug adsorption. *Int J Pharm* 2016;**514**:212. 9.
32. He YZ, et al. Drug nanoclusters formed in confined nano-cages of CD-MOF: dramatic enhancement of solubility and bioavailability of azilsartan. *Acta Pharm Sin B* 2019;**9**:97−106.
33. Kaye RS, Purewal TS, Alpar OH. Development and testing of particulate formulations for the nasal delivery of antibodies. *J Control Release* 2009;**135**:127. 35.
34. Zhu JH, Lee HP, Lim KM, Lee SJ. Evaluation and comparison of nasal airway flow patterns among three subjects from Caucasian, Chinese and Indian ethnic groups using computational fluid dynamics simulation. *Respir Physiol Neurobiol* 2011;**175**:62. 9.
35. Zang HR, Liu YX, Zhang L, Wang T, Li LF, Wu J. Nasal cavity computer fluid dynamics analysis on 60 healthy Chinese adults. *Chin J Otorhinolaryngol Head Neck Surg* 2013;**48**:814. 7.
36. Ayoub MRR, Lethem MI, Lansley AB. The effect of ingredients commonly used in nasal and inhaled solutions on the secretion of mucus. *in vitro*. *Int J Pharm* 2021;**608**:121054. 65.
37. Liu N, et al. Highly reliable transparent superhydrophobic composite by organosilane/denture base resin-modified alkylated silica nanoparticles against contaminants. *Surface Interfac* 2022;**35**:102460. 67.
38. He SY, et al. Metal-organic frameworks for advanced drug delivery. *Acta Pharm Sin B* 2021;**11**:2362. 95.
39. Sosnowski TR, Rapiejko P, Sova J, Dobrowolska K. Impact of physicochemical properties of nasal spray products on drug deposition and transport in the pediatric nasal cavity model. *Int J Pharm* 2020;**574**:118911. 20.